Stefanie Tofelde | Aaron Bufe | Jens Turowski

Hillslope Sediment Supply Limits Alluvial Valley Width

Suggested citation referring to the original publication:
AGU Advances (2022), pp. 1 - 20
DOI https://doi.org/10.1029/2021AV000641
ISSN 2576-604X

Journal article | Version of record

Secondary publication archived on the Publication Server of the University of Potsdam:
Zweitveröffentlichungen der Universität Potsdam :
Mathematisch-Naturwissenschaftliche Reihe 1289
ISSN: 1866-8372
https://nbn-resolving.org/urn:nbn:de:kobv:517-opus4-572879
DOI: https://doi.org/10.25932/publishup-57287

AGU Advances

RESEARCH ARTICLE
10.1029/2021AV000641

Hillslope Sediment Supply Limits Alluvial Valley Width

Stefanie Tofelde[1], Aaron Bufe[2], and Jens M. Turowski[2]

[1]Institute of Geosciences, University of Potsdam, Potsdam, Germany, [2]Helmholtz Zentrum Potsdam, GeoForschungsZentrum (GFZ) Potsdam, Potsdam, Germany

Key Points:

- Valley width in alluvial terraces is inversely proportional to valley height
- We suggest sediment supply from river-independent hillslope erosion limits valley width
- The coupling of hillslopes and river channels demands revision of current valley-evolution models

Supporting Information:

Supporting Information may be found in the online version of this article.

Correspondence to:

S. Tofelde,
tofelde@uni-potsdam.de

Citation:

Tofelde, S., Bufe, A., & Turowski, J. M. (2022). Hillslope sediment supply limits alluvial valley width. *AGU Advances*, *3*, e2021AV000641. https://doi.org/10.1029/2021AV000641

Received 17 DEC 2021
Accepted 12 SEP 2022

Peer Review The peer review history for this article is available as a PDF in the Supporting Information.

Author Contributions:

Conceptualization: Stefanie Tofelde, Aaron Bufe, Jens M. Turowski
Investigation: Stefanie Tofelde
Methodology: Stefanie Tofelde, Aaron Bufe, Jens M. Turowski
Visualization: Stefanie Tofelde
Writing – original draft: Stefanie Tofelde, Aaron Bufe, Jens M. Turowski

Abstract River-valley morphology preserves information on tectonic and climatic conditions that shape landscapes. Observations suggest that river discharge and valley-wall lithology are the main controls on valley width. Yet, current models based on these observations fail to explain the full range of cross-sectional valley shapes in nature, suggesting hitherto unquantified controls on valley width. In particular, current models cannot explain the existence of paired terrace sequences that form under cyclic climate forcing. Paired river terraces are staircases of abandoned floodplains on both valley sides, and hence preserve past valley widths. Their formation requires alternating phases of predominantly river incision and predominantly lateral planation, plus progressive valley narrowing. While cyclic Quaternary climate changes can explain shifts between incision and lateral erosion, the driving mechanism of valley narrowing is unknown. Here, we extract valley geometries from climatically formed, alluvial river-terrace sequences and show that across our dataset, the total cumulative terrace height (here: total valley height) explains 90%–99% of the variance in valley width at the terrace sites. This finding suggests that valley height, or a parameter that scales linearly with valley height, controls valley width in addition to river discharge and lithology. To explain this valley-width-height relationship, we reformulate existing valley-width models and suggest that, when adjusting to new boundary conditions, alluvial valleys evolve to a width at which sediment removal from valley walls matches lateral sediment supply from hillslope erosion. Such a hillslope-channel coupling is not captured in current valley-evolution models. Our model can explain the existence of paired terrace sequences under cyclic climate forcing and relates valley width to measurable field parameters. Therefore, it facilitates the reconstruction of past climatic and tectonic conditions from valley topography.

Plain Language Summary Little is known on how valleys widen and what sets their width. Therefore, it remains difficult to model the wealth of valley geometries that occur in nature and to predict how valleys adjust to environmental changes. Paired river terraces are staircases of abandoned valley floors that preserve valley widths of the past. The formation of river-terrace sequences requires changes between vertical river incision and lateral river erosion of valley walls. Moreover, to preserve terraces on both sides of the river, the valley has to narrow over time. While cyclic climate changes during the Quaternary can explain the alternations between vertical incision and lateral erosion, they cannot explain why those valleys narrow. Here we investigate past valley geometries in paired, climatically formed river terraces. We find a negative linear relationship between valley width and valley height. We propose that this relationship reflects a balance between sediment that is moved from hillslopes into the channel and the capacity of the river to remove this sediment. Higher valley walls contribute more sediment that protects the wall from further widening. By including this hillslope-erosion term, valley-formation models can reproduce paired river terraces, and allow us to work toward "reading" climatic conditions from valley geometries.

1. Introduction

River valleys set the relief of eroding landscapes, control the habitat and distribution of many species, and influence the direction of nutrient and water fluxes across large parts of Earth's surface (Hilton & West, 2020; Macklin & Lewin, 2015; May et al., 2013). The range of valley widths and depths that occur on Earth spans from meters to multiple kilometers, and constraining processes and controls on the formation of river valleys is a key component of understanding landscape development (Perron et al., 2009; Tucker & Slingerland, 1997; Willett et al., 2014). River valleys evolve by deepening through vertical river incision and widening through lateral erosion of valley walls (Figure 1). Whereas much emphasis has been put on investigating processes and rates of vertical incision (e.g., Tucker & Slingerland, 1997; Tucker & Whipple, 2002), our limited knowledge on parameters controlling valley widening and valley-bottom width prevents us from interpreting the range of valley geometries that occur

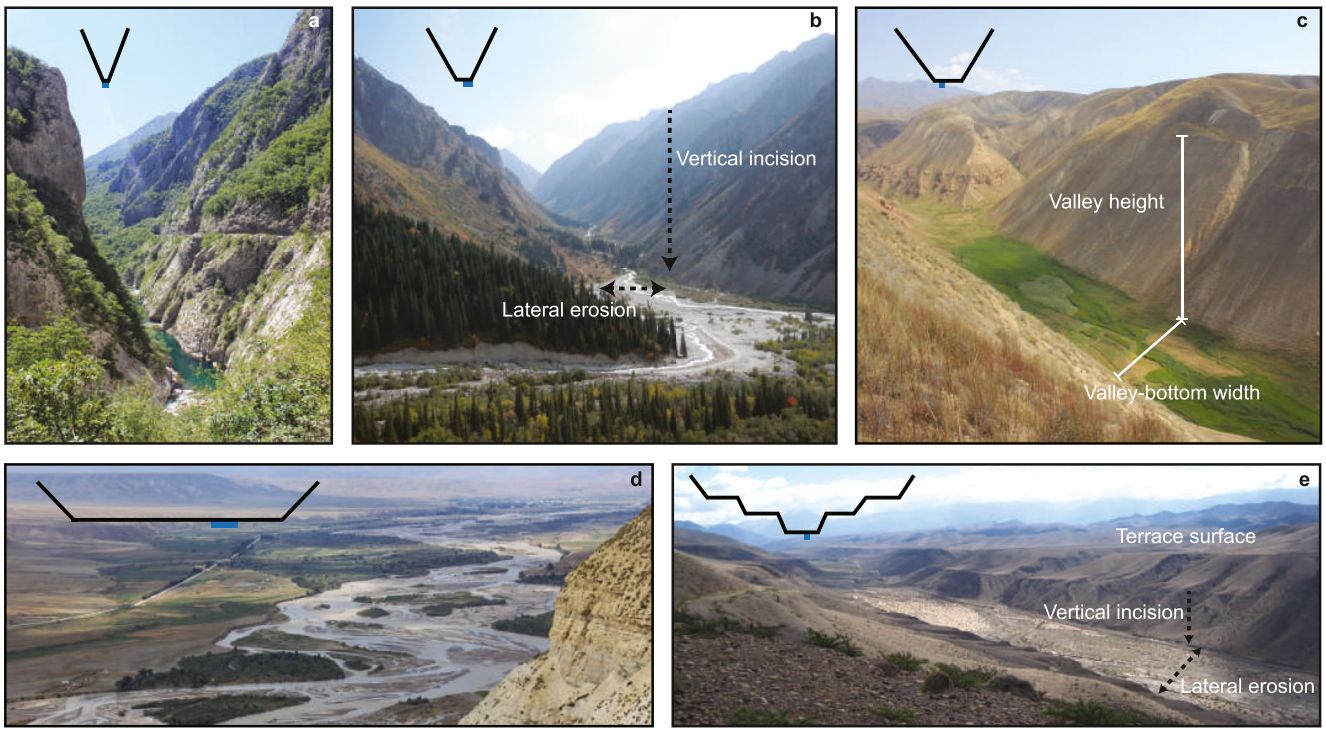

Figure 1. Field photos and schematic illustration of natural cross-sectional valley shapes. Valleys widen when river channels move laterally and erode valley walls. Valley-bottom width can evolve to several times the width of rivers flowing through them. River width is indicated by the blue bar. (a) Morača river, Montenegro; (b) Ala-Artscha river, Kirgizstan; (c) tributary to Naryn river, Kirgizstan; (d) Naryn river, Kirgizstan; (e) alluvial terrace sequence in the Toro river, Argentina. Solid white lines indicate distances, dashed black arrows show processes or rates.

in nature and predicting how valleys evolve under changing environmental conditions (Langston & Tucker, 2018; Marcotte et al., 2021).

A geomorphic feature that can be observed in many river valleys around the world are river-terrace sequences (Figure 1e). River-terrace sequences are staircases composed of flat surfaces (treads) and steep walls (risers) that are either carved into previously deposited river sediments (alluvial terraces, Figure 1e) or bedrock (strath terraces). In contrast to the common V-shape river valleys (Figure 1a), terrace sequences have the advantage of preserving information on past valley geometries. V-shape river valleys form where net river incision triggers over-steepening of the river-adjacent hillslopes, and subsequent hillslope adjustment (Figure 2a; e.g., Ahnert, 1998; Hurst et al., 2012). Constant hillslope adjustment, however, erases information on past valley widths. In contrast, river terraces form when phases of river incision are interrupted by prolonged phases of

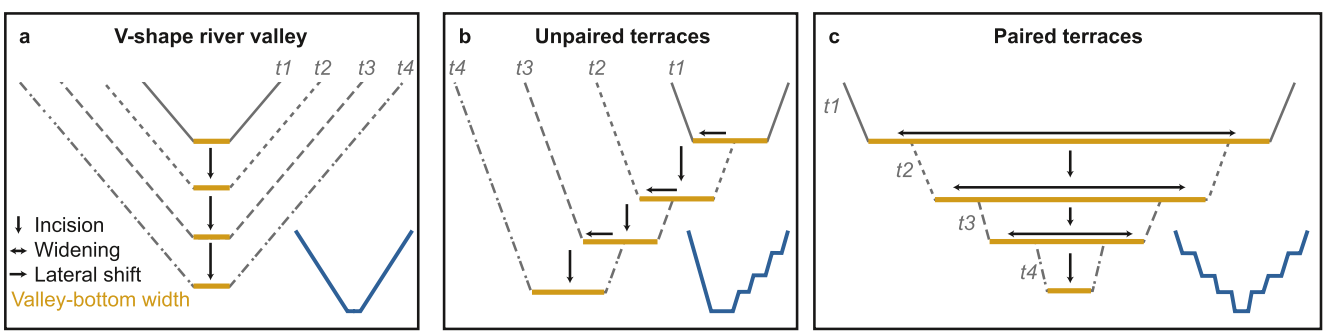

Figure 2. Schematic summary of valley forming processes resulting in different valley shapes. (a) Common V-shape river valleys only require net river incision, which results in constant adjustment of the hillslopes and valley width at higher elevations. The active valley-bottom width (brown) can be constant through time. (b) Unpaired terraces can form when phases of river incision are interrupted by lateral planation with a net lateral shift in the active valley bottom. (c) Paired terraces can only form when incision phases are interrupted by lateral planation and valley widening, but with an overall reduction in valley-bottom width. t = time.

terrace-tread planation through lateral erosion of valley walls (Figures 2b and 2c) (Bridgland & Westaway, 2008; Bull, 1990; Gilbert, 1877; Hancock & Anderson, 2002; Pazzaglia, 2013). Here, part of the valley bottom is preserved, even after subsequent phases of incision and lateral erosion (Figures 2b and 2c). Importantly, where river terraces are paired, the width of valleys that formed at different points in time can be estimated from the terrace pairs (Figure 2c). Therefore, these sequences present exceptional records to test valley-formation models.

The creation of an entire terrace sequence requires repeated alternations in the ratio of vertical incision to lateral erosion (Bridgland & Westaway, 2008; Bull, 1990; Gilbert, 1877; Hancock & Anderson, 2002; Li et al., 2021; Pazzaglia, 2013). Such alternations can be caused by variations in either upstream water and sediment supply or alternations in downstream base-level elevation (Baynes et al., 2018; Bull, 1990; Frankel et al., 2007; Hancock & Anderson, 2002; Lane, 1955; Merritts et al., 1994; Scherler et al., 2015; Tofelde et al., 2019). Therefore, Quaternary river-terrace sequences all around the world are oftentimes associated with cyclic climate changes, in particular glacial-interglacial transitions (Bridgland & Westaway, 2008; Maddy et al., 2001; Schanz et al., 2018; Tao et al., 2020; Van den Berg & van Hoof, 2001; Vandenberghe, 2002). In addition to repeated alternations in the ratio of vertical incision to lateral erosion, terrace sequences can only form when the width to which a valley widens is laterally offset with respect to the previous terrace level. In unpaired terraces, where treads are only preserved on one valley side, the lateral offset between terrace levels can be caused by a laterally moving active-channel belt (Figure 2b). In contrast, the formation of paired terraces, with treads being preserved at similar elevations on both valley sides, necessitates a reduction in valley width with each incision phase (Figure 2c). It is unclear how cyclic climate changes of approximately constant amplitude and wavelength during the Quaternary (Lisiecki & Raymo, 2005) can systematically lead to a reduction in valley width. And current valley-formation models fail to reproduce paired terrace sequences formed under cyclic climate forcing. Thus, either these terraces form under a particular set of conditions that is not covered by current models, or the models are missing parameters or interactions that are important for valley formation generally.

Taken together, river-terrace sequences preserve valley widths and could be used to test valley-formation models in ways that are impossible in V-shaped valleys. However, the reasons for the progressive valley narrowing, which is necessary to preserve paired river-terrace sequences, are poorly understood. Here, we investigate valley-width evolution preserved in river-terrace sequences, and discuss which valley-width-control parameters can best explain the required reduction in valley width. We propose a new valley-widening model, and speculate on its applicability to valleys that do not preserve terraces.

2. Parameters Controlling Valley Width

Valley-bottom width describes the distance along the sub-horizontal plane between two adjacent inclined hillslopes within a valley cross section that is regularly reworked by the active river (Figure 1). Field studies found that valley bottoms grow wider in softer lithologies and with greater river-water discharge (Brocard & Van der Beek, 2006; Langston & Temme, 2019; Limaye, 2020; Montgomery, 2002; Schanz & Montgomery, 2016; Suzuki, 1982; Tomkin et al., 2003). However, for a given lithology and discharge, valley widths scatter up to an order of magnitude (Brocard & Van der Beek, 2006; Langston & Temme, 2019; Schanz & Montgomery, 2016). This scatter indicates that at least one other parameter exerts an important control on valley width.

Existing models of valley widening have been developed based on analogue and numerical experiments (Bufe et al., 2019; Hancock & Anderson, 2002; Langston & Tucker, 2018; Martin et al., 2011), but they have rarely been systematically tested against natural valley geometries (exception see Langston & Temme, 2019). Widening a valley requires the erosion of valley walls, and valley width, W [L], has most commonly been described as a function of a widening rate (i.e., the increase in valley width per unit time, dW/dt [L T^{-1}]) integrated across the duration of widening (Hancock & Anderson, 2002; Mackin, 1937; Suzuki, 1982). In these models, the valley width is transient and evolves asymptotically through time (Figure 3a). The widening rate is commonly parameterized as:

$$\frac{dW}{dt} = E_R P, \tag{1}$$

where P [−] is the fraction of time that the river is in contact with the valley wall (Blum et al., 2013; Hancock & Anderson, 2002; Martin et al., 2011), and E_R [L T^{-1}] is the wall-erosion rate by the river in times of wall contact

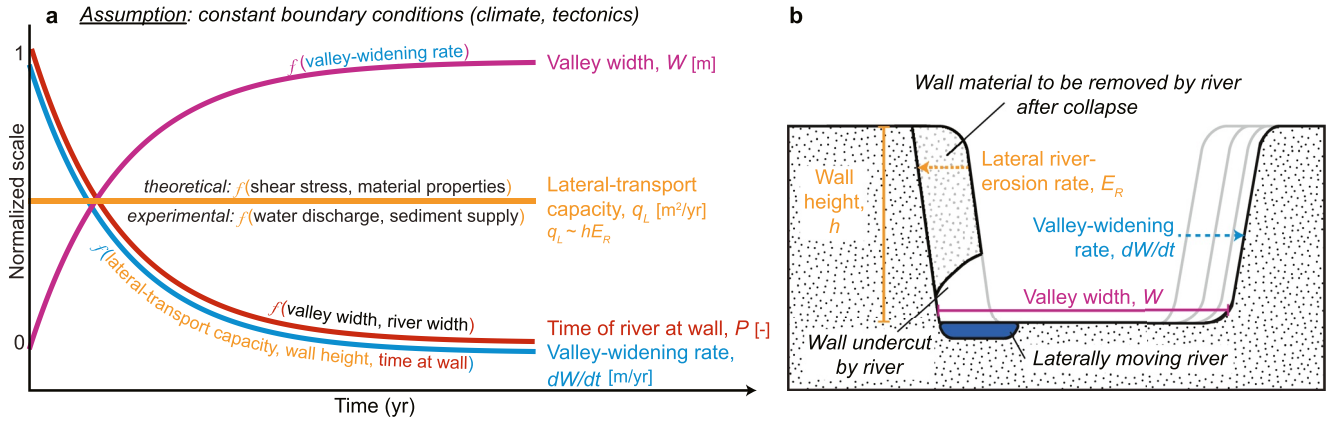

Figure 3. Current model of valley-width evolution (a) through time and (b) in cross-sectional view. Rivers widen valleys by undercutting the adjacent wall, which triggers wall collapse and the formation of a sediment pile at the wall toe that protects the wall from further lateral erosion until the sediment pile is removed by the river. The amount of sediment that can be removed by the river (lateral-transport capacity) is thought to depend on boundary conditions (water discharge, channel slope, lithology, cohesion of wall material, etc.), and thus is constant as long as boundary conditions are constant. If the lateral-transport capacity is constant, the rate at which the wall retreats scales linearly with wall height. As a valley widens, the river spends less time at valley walls, and the valley-widening rate decreases.

(Figure 3a). Rivers are typically thought to widen a valley by undercutting their adjacent walls (Langston & Tucker, 2018; Malatesta et al., 2017; Martin et al., 2011) (Figure 3b). Particularly in unconsolidated sediment (alluvium), undercutting causes wall collapse and the formation of a talus pile that has to be removed to further widen the valley. The lateral wall-erosion rate by the river, E_R, has, therefore, been suggested to scale with the height of the valley wall that is actively eroded, h [L] (Blum et al., 2013; Bufe et al., 2019; Malatesta et al., 2017; Martin et al., 2011), and the capacity of the river to erode and transport material laterally per unit length of the river (lateral-transport capacity, q_L [L^2 T^{-1}]) (Bufe et al., 2019; Martin et al., 2011) (Figure 3a), such that

$$E_R = \frac{q_L}{h}. \tag{2}$$

Hence, for a given lateral-transport capacity (constant volume of material that can be removed per time), high walls result in low lateral erosion rates and low walls in higher lateral erosion rates (Bufe et al., 2016, 2019; Langston & Tucker, 2018; Malatesta et al., 2017; Martin et al., 2011). The lateral-transport capacity, q_L, is commonly described in numerical models by a combination of shear stress or stream power exerted on the valley wall and wall-material properties (lithology, cohesion, etc.) (Finnegan & Dietrich, 2011; Hancock & Anderson, 2002; Howard & Knutson, 1984; Langston & Tucker, 2018; Limaye & Lamb, 2014; Martin et al., 2011), and has been shown to scale with upstream water discharge and sediment supply in physical experiments (Bufe et al., 2019; Wickert et al., 2013) and field studies (Constantine et al., 2014; Dunne et al., 2010). The fraction of time P that a laterally moving river is in contact with any of its two walls has been quantified as a ratio of river width, w_r [L], and valley width, and hence decreases when valleys widen (Hancock & Anderson, 2002; Martin et al., 2011) (Figure 3a). Taken together, we obtain the formulation proposed by Martin et al. (2011) and simplified by Blum et al. (2013) to:

$$\frac{dW}{dt} = E_R P = \frac{q_L}{h}\frac{w_r}{W}. \tag{3}$$

Based on this current understanding, a reduction in valley width with each incision step that is necessary to form paired terrace sequences can be achieved either by:

1. A decrease in widening duration, t, with each incision phase;
2. A decrease in the widening rate, $\frac{dW}{dt}$, with each incision phase through either (a) a reduction in the lateral-transport capacity q_L (e.g., water discharge, sediment supply, changes in material properties) or (b) an increase in the wall height h; or
3. A so far unknown control parameter on valley width.

In this study, we analyze valley width in paired, climate-driven terrace sequences that formed over several Quaternary climate-cycles. We focus our analysis on alluvial terraces to ensure relatively homogenous wall material

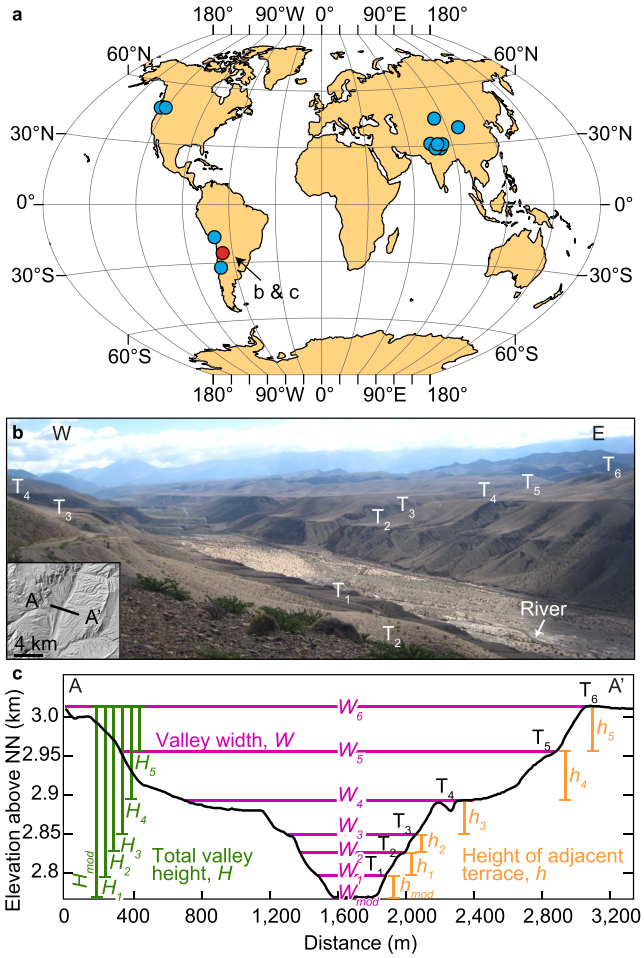

Figure 4. Terrace compilation and analysis. (a) Global distribution of the 12 analyzed alluvial terrace sequences as given in Table 1. Red circle points to locations of one exemplary cross section shown in detail in (b) and (c). (b) Field photo of the terrace sequence in the Quebrada del Toro, NW Argentina, 24°30′S and 65°50′W. (c) Cross section of the terrace sequence in the Quebrada del Toro as seen in (b) extracted from the TanDEMX digital elevation model. Colored lines indicate extracted length of valley width, *W*, height of the adjacent terrace, *h*, and total valley height, *H*. Terrace names are according to Tofelde et al. (2017).

properties compared to terraces cut into bedrock. Quaternary climate cycles have displayed comparable amplitudes and periods, and are not characterized by a systematic reduction in the duration of individual climate phases (Lisiecki & Raymo, 2005). Moreover, the investigated terrace sequences formed over times longer than a single warming or cooling phase. Consequently, we consider a systematic step-wise reduction in widening duration (option 1) or decrease in lateral-transport capacity (option 2a) as unlikely to explain all investigated terrace sequences. Instead, we hypothesize that paired terrace sequences form due to an unknown feedback with the wall height and will focus on the role of wall height in terrace formation (option 2b). For comparable widening durations and lateral-transport capacities (which include wall-material properties), Equation 3 predicts that valley width should scale with the height of the wall that is actively undercut by the channel (i.e., lower-most terrace) as $W \propto \sqrt{\frac{1}{h}}$.

Although we particularly test the role of wall height, we will discuss each of the options above as a potential explanation for paired terrace formation (see Section 5).

3. Methods

3.1. Extraction of Field Data

To test the relationship between terrace height and valley width, we globally compiled alluvial terrace sequences that have been associated with late Quaternary climate changes (Figure 4a, Table 1). All terrace cross sections that are accepted in our compilation (a) include both valley sides, (b) show absolute values of distance and height, as well as profile location, and, (c) display a minimum of three terrace levels out of which at least one is preserved as a paired terrace at the profile location. A minimum of three terrace levels is required to generate at least three width-height data points for regression analysis. Twelve terrace sequences with between three and eight terrace levels obeyed these criteria. The cross section of the terrace sequence in the Quebrada del Toro, NW Argentina (Figure 4b; Tofelde et al., 2017) was extracted from the TanDEMX digital elevation model (Research agreement, see acknowledgments) with a horizontal resolution of 1 arcsec or ∼12 m. The other 11 cross sections were taken from eight publications (Bookhagen et al., 2006; Colombo et al., 2000; Hu et al., 2017; Pazzaglia & Brandon, 2001; Poisson & Avouac, 2004; Ray & Srivastava, 2010; Rigsby et al., 2003; Wang et al., 2017). From the cross sections and for each terrace level, we measured valley width, *W*, height of the adjacent terrace wall, *h*, as well as the height of the entire terrace sequence or total valley height, *H*, in Adobe Illustrator (Figure 4c). In case of unpaired terraces, valley width was measured where the tread elevation hits the opposite wall, thus giving a maximum valley width. Terrace height in unpaired terraces was determined on the preserved terrace only, because wall height during widening times on the other side cannot be reconstructed. We note that in many terrace sequences, not all individual terraces within each sequence are preserved as paired terraces at the profile location, but in some cases can be traced to paired terraces upstream or downstream. To ensure that we only include terrace sites that reliably preserve information on past valley widths, we avoided purely unpaired terrace sequences, for which valley widths are modified through time (Figure 2b). Instead, we only included cross sections that contain paired terrace levels and clearly indicate a reduction in valley width at some point during terrace formation (Figure 2c). Measured values of *W*, *h*, and *H* were converted to true length scales based on reference measurements along the axes (Data Set S1; Tofelde et al., 2022). The topmost terrace was not displayed in all cross sections. Consequently, *H* could not be extracted from such terrace sequences. In those cases, we determined *H* with respect to a chosen reference surface within the terrace sequence. This approach reduces all *H* measurements within one terrace sequence by the same amount and thus does not affect the relative height

Table 1
Details on the 12 Analyzed Terrace Cross Sections

Author	Year	Place	Latitude (°)	Longitude (°)	NoT	A (km^2)	Figures in original publication
Wang et al. (A)	2017	Sutlej River, Tibet	31.09	80.8	8	9,113	Figure 3a
Wang et al. (C)	2017	Sutlej River, Tibet	31.13	80.73	6	9,113	Figure 3c
Bookhagen et al.	2006	Sutley river, India	31.3892	77.6256	6	48,431	Figure 4
Colombo et al.	2000	Albarracín Fan, San Juan River, Argentina	−31.5472	−68.8385	3	116	Figure 4
Hu et al.	2017	Dahe river, Quilian Shan, Tibet	39.0751	99.4841	5	78	Figure 4b
Poisson and Avouac	2004	Kuitun river, Tien Shan, China	44.1845	84.7706	4	1,958	Figure 4b
Pazzaglia and Brandon (B)	2001	Clearwater Basin, Olympic Peninsula, USA	47.6009	−124.2837	3	358	Figure 8b
Pazzaglia and Brandon (C)	2001	Clearwater Basin, Olympic Peninsula, USA	47.6512	−124.2055	4	249	Figure 8c
Ray and Srivastava (1)	2010	Alaknanda (Gholtir), India	30.3006	79.0925	3	8,600	Figure 12 Gholtir
Ray and Srivastava (2)	2010	Alaknanda (Gaucher), India	30.2937	79.151	5	8,331	Figure 12 Gaucher
Rigsby et al.	2003	Río Ilave, Peru	−16.1142	−69.6706	4	9,957	Figure 7 Huancumiri
Tofelde at al.	2017	Río Toro, Argentina	−24.5062	−65.8635	6	1,673	This study Figure 4

Note. NoT = number of terraces at profile location. This number is not always equivalent to the number of analyzed datapoints, for example, when the width of the uppermost terrace could not be reconstructed. Figure number indicates the analyzed figure in the original publication.

differences between terraces, only the absolute height value H. In three cross sections (Poisson & Avouac, 2004; Wang et al., 2017), the width of the modern floodplain could not properly be identified in the provided cross sections. Floodplain width for the two profiles in Wang et al. (2017) were estimated from Google Earth. For the cross section in Poisson and Avouac (2004), we only extracted the width and height values of the terraces >6 ka, because the authors inferred a substantial change in discharge conditions post 6 ka, thus violating our assumptions of comparable lateral-transport capacities.

3.2. Methodological Uncertainties

Deviations of measured length and width values from true initial values can be introduced in three ways. First, limited resolutions of cross sections or simplifications of the cross section by authors in the original publication could introduce uncertainty in length measurements. Hu et al. (2017) published the measured heights of five terrace levels between 93 and 3 m above the modern Dahe River on which the cross section was based. The maximum difference between the published heights and the height values that we reconstructed from the published cross section is 1.2 m. The average offset is below 10% (Data Set S1; Tofelde et al., 2022). Bookhagen et al. (2006) published four absolute terrace heights between 120 and 10 m. Heights extracted from the cross section and heights given by the authors differ by less than 10%, apart from the lowest terrace with a measured height of 13.9 versus 10 m as given by the authors. In total, for 7 out of 12 terrace cross sections terrace heights were provided in the original publication (Data Set S1; Tofelde et al., 2022). Height values stem mostly from direct measurements in the field. The comparison between terrace heights measured in the field and extracted from cross sections shows that our approach is overall able to reconstruct terrace heights (Figure S3 in Supporting Information S1) and that the information loss by extracting values from the cross-section figures results in uncertainties on the order of ∼10%.

Second, unpaired terraces only partially preserve past valley geometries. On the valley side without preserved terraces, measurements of valley width might be overestimated, such that all valley widths are maximum values. Terrace heights were only measured on the preserved terrace side. Hence, this height value underestimates the wall height on the opposite side which has to be moved to widen the valley. According to theory, a higher terrace wall would result in lower lateral wall-erosion rates by the river (Equation 3), and therefore narrower valleys. As such, valley geometry reconstructions from unpaired terraces might violate the expected W-h relationship. We take this potential bias into account when discussing the results (see Section 5.1.2). Even though some terraces are not preserved as paired terraces right at the profile location, they can oftentimes be traced to paired terraces further upstream or downstream.

Third, modification of terrace geometries after terrace-surface abandonment due to erosion, sediment deposition or by humans can impact terrace width-height relationships. A theoretical horizontal terrace-wall retreat rate of 0.5 mm/yr would result in a 5 m retreat of a 10,000-year-old terrace or a 50 m retreat of a 100,000-year-old terrace. A horizontal retreat rate of 0.1 mm/yr would result in the horizontal loss of 1 and 10 m for 10,000 or 100,000-year-old terraces, respectively. These values are mostly within measurement uncertainties considering that the majority of older terraces relate to valley widths of more than 1,000 m. We conclude that measurement uncertainties, partial preservation and modification of terrace geometries over time affect the terrace width and height measurements, but they most likely do not substantially change the overall width-depth relationships.

3.3. Data Quality

Our data set is a compilation of previously published terrace cross sections. For our specific purpose, the 12 data sets are of different quality and reliability. Therefore, we qualitatively subdivide the data in seven more reliable and five less reliable cross sections based on (a) the quality of the cross section, (b) constraints on the terrace-formation mechanism (climatically and not tectonically or autogenically formed), and (c) alluvial-terrace type (fill- and not fill-cut terraces, bedrock component; Bull, 1991) (Table S1 in Supporting Information S1). A terrace data set was qualified as lower quality if it failed a quality check in at least one of three categories. First, cross-section quality was evaluated based on the source of the data set and how detailed the assessment of the cross section was reported. A data set was regarded as low quality in this category if the cross section was constructed from a topographic map or if no details on cross-section assessment were provided (Table S1 in Supporting Information S1). Second, we evaluated the ability to identify climatic changes as the main driver of terrace formation. Here, we followed the interpretation of the authors in the original publication. A data set was regarded as low quality if the formation of the terrace cross section could not unambiguously be related to climatic changes (Table S1 in Supporting Information S1). Third, we assessed the likelihood for the presence of cut-fill terraces (Bull, 1991) that complicate the interpretation of terrace sequences. Both fill terraces and cut-fill terraces are formed by river incision into previously deposited sediment. Fill terraces mark a change from aggradation or stable conditions to incision, and a series of fill terraces represent cycles of aggradation and incision. Instead, series of cut-fill terraces can be carved into a single valley fill as the river incises. Importantly, these terraces can form autogenically during short phases of planation under a constant climate (Malatesta et al., 2017), and they do not necessarily reflect climatic cycles. Thus, we consider fill terraces as more reliable for our purpose. Sequences for which the presence of cut-fill terraces are likely were deemed lower quality in this third category (Table S1 in Supporting Information S1). Note that phases of aggradation during fill-terrace formation result in a decrease of the height of the river adjacent terrace, h. However, as long as the duration of aggradation, widening, and incision is comparable between terrace sequences, the predicted scaling of $W \propto \sqrt{\frac{1}{h}}$ should still hold true. In addition, two of the cross sections have a bedrock component on one valley side (Bookhagen et al., 2006; Ray & Srivastava, 2010), and are therefore considered as less reliable.

3.4. Regression Analysis of Field Data

In order to test for the hypothesized valley width and terrace height relationship, we performed a regression analysis by fitting the following equation to all 12 data sets:

$$W = a\sqrt{\frac{1}{h}} + b. \tag{4}$$

In addition, linear regressions between valley width, W, and height of the adjacent terrace, h, as well as total valley height, H, were performed.

In order to evaluate the regressions, we calculated the goodness-of-fit (ordinary R^2) and the adjusted R^2. The adjusted R^2 value is interpreted equivalent to the ordinary R^2 value, but takes the number of observations and the number of regression coefficients into account. In order to investigate whether the ordinary R^2 value is biased with respect to the number of datapoints, we compare the ordinary and the adjusted R^2 value. However, we do not observe any systematic trend in either ordinary R^2 or adjusted R^2 value with the number of datapoints (number

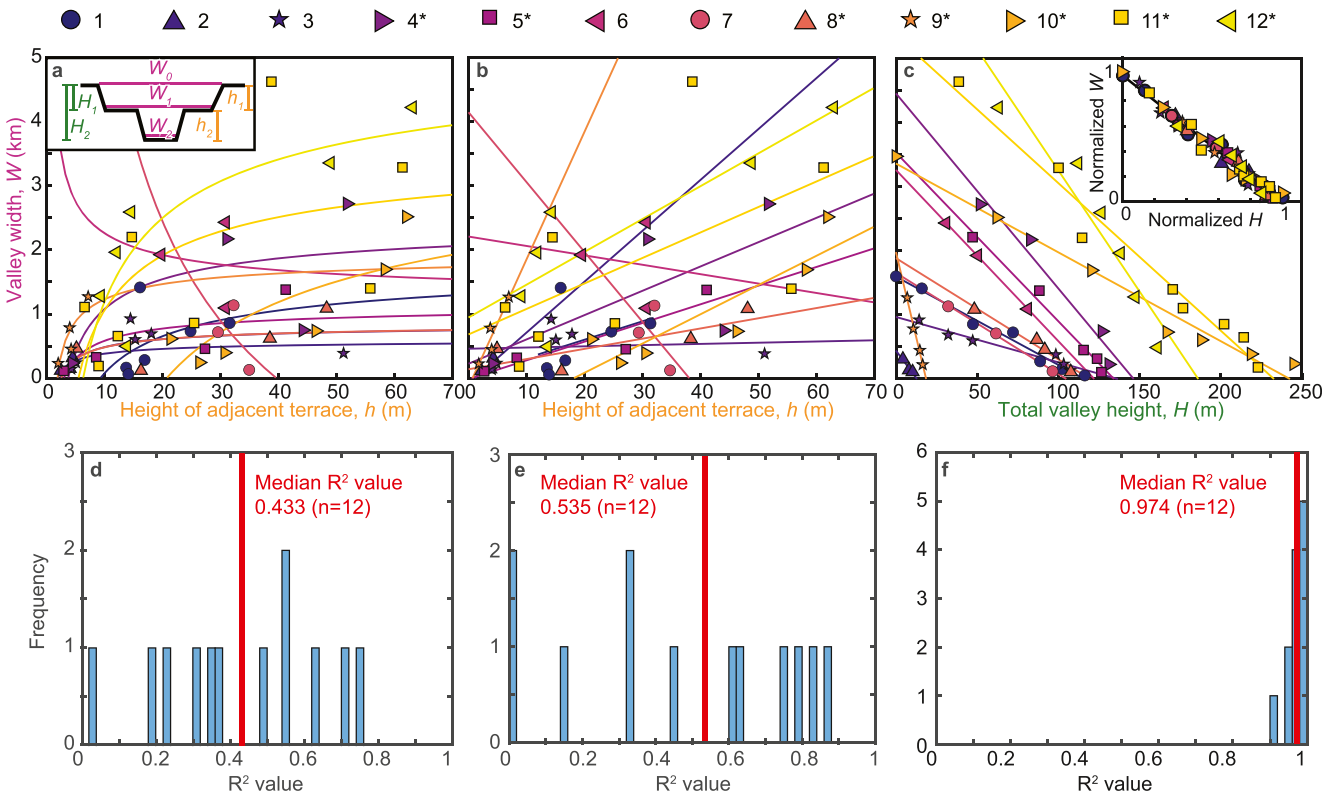

Figure 5. Field data of terrace height and valley width. (a) Hypothesized square-root correlation of valley width, W, and height of adjacent terrace, h (Equation 4). (b) Linear regression between W and h. (c) Correlation between valley width, W and total valley height, H. Insert shows valley width and valley height normalized by their intercept with the y-axis and x-axis of the linear regression, respectively. (d, e, and f) The frequencies of regression R^2 values for the square-root regression between W and h, the linear regression between W and h, and the linear regression between W and H, respectively. See Section 3.2 for evaluation of data uncertainty. (1) (Bookhagen et al., 2006), (2) (Colombo et al., 2000), (3) (Hu et al., 2017), (4 and 5) (Pazzaglia & Brandon, 2001), (6) (Poisson & Avouac, 2004), (7 and 8) (Ray & Srivastava, 2010), (9) (Rigsby et al., 2003), (10) (Tofelde et al., 2017), and (11 and 12) (Wang et al., 2017). Asterisk marks the most reliable datasets.

of terraces) (Figure S4 in Supporting Information S1). Therefore, we consider the ordinary R^2 value (R^2 value hereafter) as appropriate metric to compare the data sets.

4. Results

The hypothesized fit between W and h for the 12 field data sets (Figure 5a) yields R^2 values between 0.020 and 0.753, with a median of 0.433 for all 12 fits and 0.522 for the 7 most reliable terrace sequences (Figure 5d, Table S2 in Supporting Information S1). Additionally, 10 out of 12 cases show a positive correlation (wider valleys with higher adjacent walls). A linear regression between W and h results in R^2 values between 0.012 and 0.880, with a median of 0.535 (Figures 5b and 5e, Table S3 in Supporting Information S1).

We find a strong negative linear correlation between W and H (i.e., the height of the entire terrace sequence) for each of the 12 cross sections (Figure 5c). The R^2 values of a linear model lie between 0.907 and 0.9998, with a median of 0.974 for all datasets and 0.971 for the seven most reliable datasets (Figure 5f, Table S4 in Supporting Information S1). Regression slopes vary between −7.1 and −106.3, with a mean of −29.2 (Table S4 in Supporting Information S1). All datasets collapse to the same line when the individual datasets are normalized by their intercepts with the x and y-axis, respectively (Figure 5c insert). The residuals of this linear model show no systematic trend (Figure S5 in Supporting Information S1).

Taken together, the formation of paired terrace sequences necessitates that valley width decreases in each successive incision cycle. Our data suggest that valley width in alluvial terrace sequences decreases systematically, but not, as expected, with respect to the wall directly undercut by the river, h. Instead valley width seems to be linked

systematically to the height of the entire valley wall. We contend that a simple linear model is a good first-order description of the scaling between W and H.

5. Discussion

5.1. Explaining the Valley-Width-Depth Relationship

The key outcome of our data compilation is the (near-)linear relationship between valley width, W, and total valley height, H, in alluvial terrace sequences, suggesting a systematic valley narrowing. We note that "apparent" valley width in V-shape valleys would also show a linear relationship with the total valley height, H (Figure 2a). However, V-shape valleys do not necessarily preserve the actual valley width at multiple times in the past, because the entire hillslopes can adjust to the incision (Figure 2a). In contrast, higher terrace levels are isolated from modern river activity, preventing river-related changes in valley width through time. Also, V-shape valleys with a hillslope angle of ∼40° would result in a W-H linear regression slope of ∼−1.2. In contrast, our measured regression slopes between −7.1 and −106.3 translate to hillslope angles between ∼8° and 0.5°, which is much gentler than typical V-shaped valleys. They, therefore, do not represent an average angle of repose with superimposed terrace steps.

The data are inconsistent with the hypothesis that the height of the adjacent terrace wall, h,—the wall directly eroded and undercut by the river—sets the local valley width for a given discharge and lithology. We have to consider, however, that part of the poor W-h relationship might be caused by unpaired terraces within the data set. For unpaired terraces, h was determined on the valley side where the youngest terrace is preserved. The height of the wall the river had to erode on the opposite valley side was either the same height as h, in case of an initially paired terrace that was later destroyed, or higher than h, if the youngest terrace was formed only on one valley side. In the latter case, a higher wall on the opposite side would decrease valley widening rates, resulting in narrower valleys. Hence, the concerned datapoints in Figures 5a and 5b would shift downwards parallel to the y-axis. Such shifts would impact the regression parameters, but not invert the many observed positive relationships (wider valleys with higher terraces) to the expected negative relationships (the higher the wall, the narrower the valley). We note, however, that the absence of a systematic relationship between valley width and the height of the lower most terrace does not falsify the idea of terrace heights influencing the widening rate (Blum et al., 2013; Bufe et al., 2019; Malatesta et al., 2017; Martin et al., 2011). Differences in widening duration or lateral-transport capacity for each terrace level would also break down the hypothesized relationship. We propose that the observed linear reduction in valley width with valley height in alluvial terrace sequences is either (a) the result of a systematic sampling bias, (b) the result of a systematic decrease in widening duration (option 1) or lateral-transport capacities (option 2a) with each terrace level, or (c) controlled by a so far unconsidered underlying physical property or process that scales linearly with valley height (option 3).

5.1.1. Testing for a Sampling Bias

If valley width shows random natural variability, stepped sequences may emerge in a limited number of cases, and the observed relationship between valley width and height may be due to the fact that we only analyze sites of valley narrowing. In order to test for such a sampling bias, we generate synthetic terrace cross sections and investigate whether the observed scaling can be reproduced if width and height values are not controlled by a systematic process, but rather vary independently and randomly. If the observed (near-)linear scaling cannot arise from these synthetic datasets, either a reduction in widening duration or rate, or some physical process must link W to H.

We generated synthetic terrace sequences by adding phases of valley incision, each with a random valley width (Figure 6). The depth of incision and the valley width for each time step, T, were considered as stochastic variables independent from one another and from the previous time step. We tested cases where valley width and incision depth were drawn from a set of pre-defined normal distributions, and cases where valley width and incision depth evolved linearly, exponentially or with a square-root relationship through time (Figure S6 in Supporting Information S1; details below). Each set up of underlying incision-depth and width distributions was repeated for various numbers of time steps, T, (i.e., climate cycles), ranging from 3 to 30. In the example shown (Figure 6), the number of incision events, T, equals 10. A terrace of time step T_i is destroyed if valley width at any later time exceeds valley width at T_i (dark blue circles), or if younger terraces erode backward to achieve the angle of repose (40°, dashed line), thereby destroying older terraces (yellow circle). A terrace at time step T_i is preserved if valley

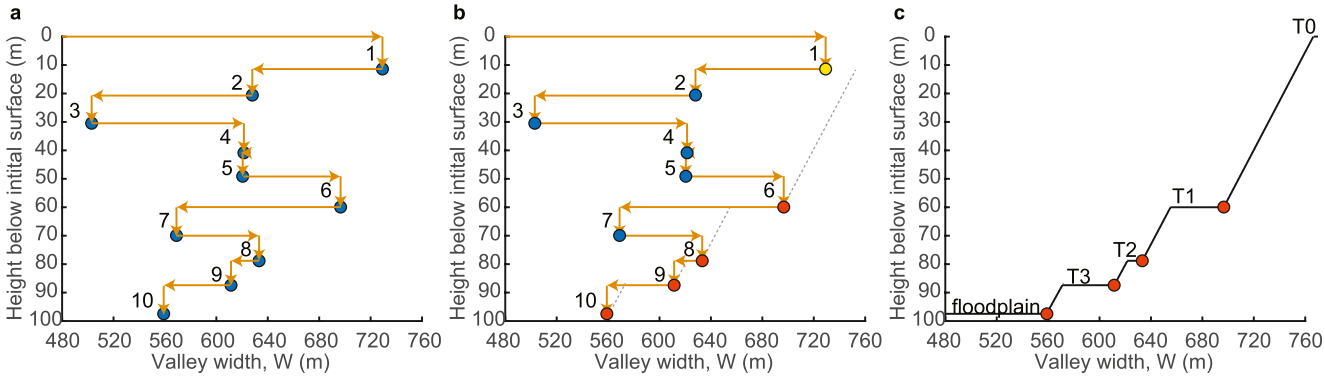

Figure 6. Model to generate synthetic datasets. For each set up, we defined two distributions from which total valley height and valley width were drawn, respectively, as well as the number of time steps, T (for details see text). (a) Here, T was set to 10 and valley width and incision depth for each time step were drawn from two normal distributions. (b) Individual terrace levels were destroyed if valley width at any following time step exceeded valley width of that given time step T (blue circles) or after backwards erosion of the terrace wall to achieve an angle of repose of 40° (yellow circle). (c) Remaining terrace levels (red circles) determine the final (half) cross section. For each set up n = 100,000 cross sections were generated.

width at all following time steps, T_{i+1}–T_{end}, is smaller after reaching the angle of repose (red circles in Figure 6). For each set up (i.e., underlying incision-depth distribution, width distribution, number of incision events, T) n = 100,000 cross sections were generated. The number of preserved terraces in most runs was less than the number of modeled time steps, because increases in valley width destroy previously formed terraces.

We treated the synthetic data equivalent to the field data. For cross sections with three or more preserved terraces, we extracted valley W-H combinations for each terrace level and performed a linear regression through each data set (examples in Figure S7 in Supporting Information S1). We compared field data and synthetic data in three ways: (a) by the number of preserved terraces, (b) by the distribution of the R^2 values resulting from the linear regressions of W versus H, and (c) by a two-sample Kolmogorow-Smirnow-test (KS-test) of R^2 value distributions. First, we compare field data to one exemplary synthetic data set in detail. Then, we discuss the comparison to all synthetic data sets more generally. In the exemplary synthetic data set, incision depth was drawn from a normal distribution with a mean and standard deviation of 10 ± 6 m and valley width from a normal distribution of 600 ± 360 m. The ratio of mean valley width to mean incision depth (i.e., terrace height) of about 60, as well as the standard deviations of 60% of the mean for both distributions, were adapted from the field data. The number of incision events, T, was set to 10.

1. The number of visible terraces in the 12 field cases ranges from 3 to 8, with a mean of 5.0 and a median of 4.5 (Figure 7a). In comparison, after 10 synthetic incision cycles, the most frequent number of preserved terraces was two in 31.6% of the sequences, followed by three (31.4%) and four (17.0%) (Figure 7b). Five or more terraces, as seen in half of the field cases, were only preserved in 6.9% of the sequences, despite 10 incision events. In 55.3% of the sequences, three or more terraces were preserved. Those cross sections with a minimum of three preserved terraces (as equivalent to field data) yield a mean of 3.6 and a median of 3 preserved terraces.
2. We fitted a linear regression to all data pairs of W and H from our synthetic terrace sequences with ≥3 levels and calculated the resulting R^2 (Figure 7c). To compare the distribution of synthetic data R^2 values with the according field data R^2 distribution, we sub-sampled the synthetic data by randomly selecting 12 out of the 55,342 R^2 values. The 12 synthetic R^2 values are compared to the 12 field cases by their medians (red lines in right column in Figure S7 in Supporting Information S1). The sub-sampling of 12 synthetic R^2 values was repeated 10,000 times. The 10,000 median R^2 values are normally distributed with a mean of 0.890 and a standard deviation of 0.048 (solid red curve Figure 7c). Hence, the median R^2 value of the field data (0.974) does not fall within one standard deviations of the median R^2 value distribution of the synthetic data, indicating the field data and synthetic data differ from one another. We also tested an alternative approach in which subsampling of twelve R^2 values from the synthetic data mirrors the number-of-terraces of the 12 field cases (Figure 7a) (three values with three terraces, three values with four terraces, one value with five terraces, etc.). The distribution of median R^2 values from 10,000 repetitions of this subsampling does not differ from the random subsampling approach, because R^2 values show no systematic trend with the number of preserved

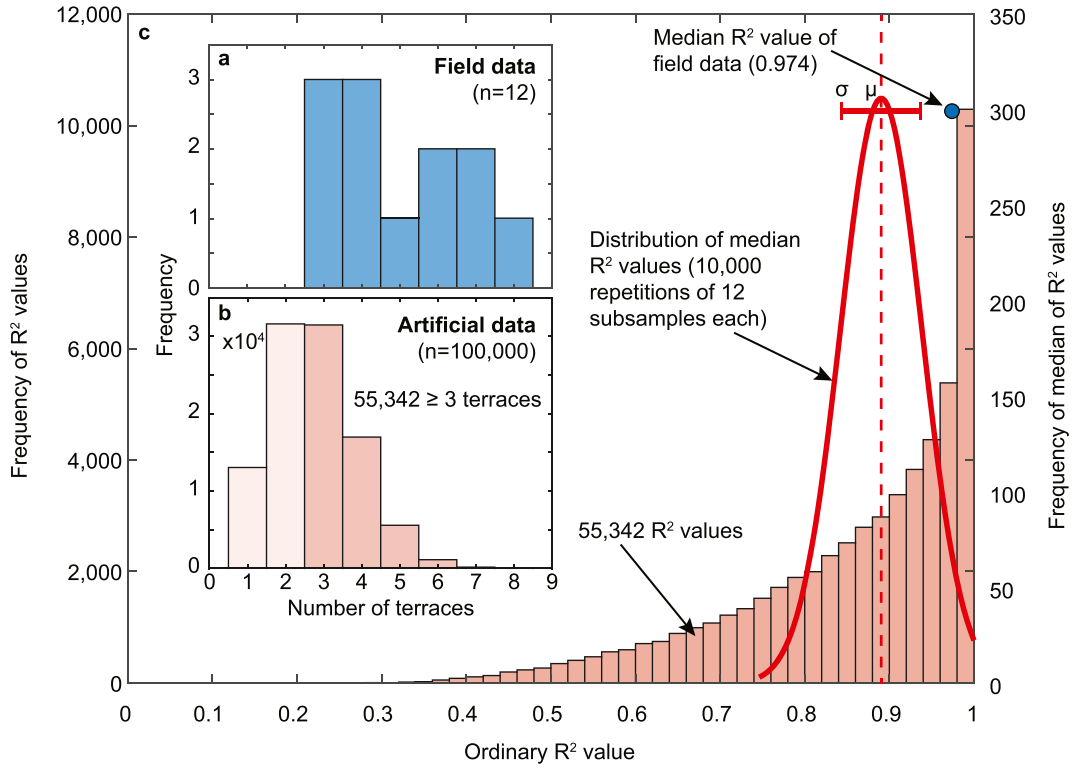

Figure 7. Results of a synthetic data set for the exemplary case of 10 climate cycles ($T = 10$). (a) The distribution of visible terraces in the 12 cross sections from field data. The median number of preserved terraces is 5. (b) The number of preserved terraces in a synthetic data set. After 10 time steps, the most abundant number of preserved terraces is two, followed by three and four. In 55.3% of the repetitive runs three or more terraces were preserved. If only the cases with three or more terraces are considered, the median number of preserved terraces is 3. (c) A histogram of R^2 values for the linear regressions between W and H for runs with a minimum of three preserved terraces ($n = 55{,}342$). Out of this distribution, a random sub-sampling of 12 R^2 values was repeated 10,000 times and the median of each distribution was calculated. The resulting 10,000 medians are nearly normal distributed with a mean and standard deviation of 0.890 and 0.048 (red curve). The median of the 12 field R^2 values (blue circle) falls outside one standard deviations.

terraces, neither for the field data (Figure S4 in Supporting Information S1) nor for synthetic data (Figure S8 in Supporting Information S1).

3. We performed a two-sample KS-test to investigate if the R^2 values from field data ($n = 12$) and synthetic data ($n = 55{,}342$) were sampled from the same underlying distribution (= null-hypothesis). The test yielded a p-value of 4.21×10^{-4} (Table S5 in Supporting Information S1) and, hence, suggests that field and synthetic data are most likely different from one another.

When keeping the underlying width and incision-depth distributions constant, while varying the number of incision events, T, from 3 to 30, the most common number of preserved terraces is two for 10 or fewer incision events and increases to three for 11 to 30 cycles (Figure S9a and Table S5 in Supporting Information S1). The medium number of preserved terraces (calculated only for cross sections with a minimum of three terraces) is three for 3 to 14 incision events and four for 15 to 30 incision events (Table S5 in Supporting Information S1). A median of 4.5 preserved terraces (as equivalent to the field data) was not obtained in any of the runs. Comparing R^2 values from field and synthetic data via the KS-test, we obtained p-values ranging from $1.2*10^{-4}$ for 30 climate cycles to 0.009 for three climate cycles (Figure S9b and Table S5 in Supporting Information S1). Hence, all synthetic datasets are different from the field data at a 1% significance level, and all but the data sets of 3 to 7 climate cycles can be distinguished at a 0.1% significance level. However, the datasets with 3 to 7 climate cycles cannot explain the field data, as some of the field sites have more terrace levels preserved (Figure 7a).

Varying the underlying distributions from which width and depth are sampled, while keeping all other parameters constant, affects the p-values of the KS-tests. Increasing the standard deviation of the normal distribution for incision depth leads to a slight reduction in p-values, in particular for runs with a low number of incision events,

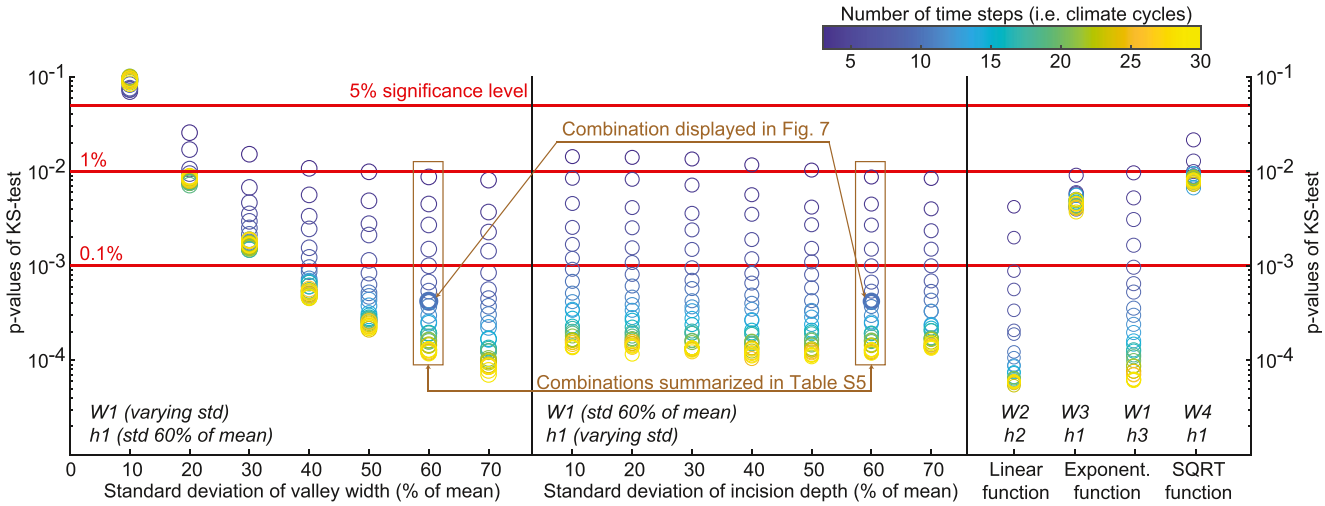

Figure 8. KS-test *p*-value results for different synthetic data sets. Synthetic cross sections were generated for a range of underlying normal distributions with variable standard deviations, and for uniform, exponential, and square-root distributions. Each set of distributions was run from three to 30 incision events. Each circle represents the comparison between the field data and 100,000 synthetic cross sections. The abbreviations *Wx* and *hx* refer to the underlying distributions. *W1, h1*: normal distributions; *W2, h2*: linear function; *W3, h3*: exponential function; W4: Squareroot function. More details are given in Figure S6 in Supporting Information S1.

T (Figure 8). Greater *p*-value differences are caused by varying the standard deviation of the valley width normal distribution. A reduction in standard deviation results in higher *p*-values. For a standard deviation of 10% (i.e., 60 m for a mean of 600 m), *p*-values lie between 0.07 and 0.1 and, thus, fall above the 5% significance level (Figure 8). However, this confinement in possible valley width values results in the destruction of most terraces, such that 70% of the generated terrace sequences have less than three terraces preserved, even for 30 incision cycles. Eight terraces, as in one of the field sites, were not created at all. In order to test for potential variability in widening or incision duration, we additionally test cases in which valley width or incision depth evolve linearly, exponentially, or with a square-root relationship through time, *t* (Figure S6 in Supporting Information S1). A square-root relationship between *W* and *t* is predicted from Equation 3. Here, we randomly sample a widening or incision duration between 1 and 20,000 years (half a ~40,000 years Milankovitch climate cycle) and calculate the corresponding *W* or *h* based on the corresponding linear, exponential or square-root function (more details in Figure S6 in Supporting Information S1). For example, when valley width and incision depth evolve linearly through time, corresponding *W* and *h* values are uniformly distributed (Figure S6 in Supporting Information S1). For the case of $T = 10$, the distribution of preserved terraces and R^2 values of the linear *W*-*H* regressions (Figure S10 in Supporting Information S1) are similar to that based on the normal distributions displayed in Figure 7. The corresponding *p*-values of the KS-tests range from 10^{-5} to 0.004 (Figure 8), pointing to a difference between synthetic and field data. Also for the exponential and square-root evolution of valley width or depth through time all *p*-values fall below the 5% significance level, and all but two cases (square-root evolution of valley width, 3 and 4 climate cycles) below the 1% significance level (Figure 8).

In summary, our simulations suggest that the strong (near-)linear correlation between *W* and *H* in the field data is unlikely to come from a random variation of width and incision depths as in the synthetic data. Hence, we reject a sampling bias as a potential explanation of the *W*-*H* relationship in observed field data and argue that either a decrease in widening rate or duration, or a physical process or parameter links valley width to total valley height.

5.1.2. Decrease in Widening Duration or Rate

A reduction in widening duration with each incision step would result in valley narrowing and potential terrace formation (Figure 3). However, a step-wise reduction in widening duration (Gilbert, 1877; Hancock & Anderson, 2002; Suzuki, 1982) is unlikely to explain the majority of the terrace sequences, especially because many terrace levels were formed over time spans exceeding a single warming or cooling phase (Bookhagen et al., 2006; Hu et al., 2017; Pazzaglia & Brandon, 2001; Tofelde et al., 2017; Wang et al., 2017), and Quaternary climate cycles do not systematically decrease in wavelength and amplitude toward the present (Lisiecki & Raymo, 2005). In addition, a reduction in widening duration can lead to valley narrowing and terrace formation, but in order to explain the observed linear *W*-*H* relationship, widening duration must decrease linearly with *H*.

We cannot think of any process linking valley height and widening duration. Hence, we conclude that a reduction in widening duration (option 1) is unlikely to be the explanation for the formation of all analyzed paired terrace sequences.

Valley narrowing can also be achieved through a reduction in the widening rate ($P\frac{q_L}{h}$), while keeping the widening duration constant. The probability of the river to be in contact with the wall, P, should scale with valley width (Hancock & Anderson, 2002), but is not thought to be impacted by valley height. The lateral-transport capacity, q_L, is thought to vary with erosive power (shear stress or stream power) of the river on the wall and wall-material properties (Finnegan & Dietrich, 2011; Hancock & Anderson, 2002; Howard & Knutson, 1984; Langston & Tucker, 2018; Limaye & Lamb, 2014; Martin et al., 2011). In constrast to terraces carved into bedrock, wall material properties are expected to be relatively constant in alluvial terrace sequences. Slight decreases in erodibility with growing valley height due to sediment overload are considered as negligible given limited total height of terrace sequences (Bruthans et al., 2014). Shear stress or stream power exerted on the wall increase with water discharge and along-river channel gradient (Hancock & Anderson, 2002; Langston & Tucker, 2018), and with planform curvature of river bends (Finnegan & Dietrich, 2011; Howard & Knutson, 1984; Langston & Tucker, 2018; Limaye & Lamb, 2014). As such, a continuous reduction in water discharge (aridification), channel gradient, or river-planform curvature would decrease the lateral-transport capacity and can potentially form a terrace sequence. While changes in the discharge regime might explain some terraces (e.g., Poisson & Avouac, 2004), it is unlikely that discharge, channel gradient or planform curvature decrease systematically with valley height in the majority of terrace sequences. The terrace sequences formed over timescales exceeding individual cooling or warming phases, thus a continuous decrease in any of those parameters is unlikely. In addition, even if a terrace sequence were formed due to a continuous reduction in the lateral-transport capacity, q_L (e.g., reduced water discharge), the resulting relationship between W and H would only be linear for comparable terrace heights, h. However, field data show great variability in terrace heights (Figure 5a). Hence, we think that a continuous reduction in lateral-transport capacities (option 2a) does not explain the formation of the paired terraces. Instead, the observed relationship between valley width and height (Figure 5c) is most likely related to a so far unmentioned parameter or process that scales about linear with valley height.

5.1.3. River-Independent Hillslope Sediment Supply

Hillslope erosion is active at all hillslope elevations and has been shown to impact the erosion behavior of rivers (Malatesta et al., 2017; Shobe et al., 2016; Wickert & Schildgen, 2019). In case of terrace sequences, the river only directly interacts with the lower-most terrace, while upper terrace levels are isolated from the river. Hence, we suggest that the missing parameter scaling linearly with total valley height is river-independent hillslope erosion. Here, we propose a new model for valley width that reproduces the observed negative linear scaling between valley width and valley height. Similar to existing valley-widening models (Blum et al., 2013; Martin et al., 2011), we assume valley widening is a function of two opposing processes: (a) the ability of the river to remove laterally supplied sediment to drive further widening, described by the product of q_L and P (Blum et al., 2013; Hancock & Anderson, 2002; Martin et al., 2011), and (b) lateral sediment supply preventing further widening, q_s (Figure 9a). In contrast to previous models, we assume that q_s is not only derived from active river erosion of the adjacent wall in times of river-wall contact, described by the product $E_R hP$ (Blum et al., 2013; Malatesta et al., 2017; Martin et al., 2011), but in addition from river-independent hillslope-erosion processes. The river-independent hillslope-erosion rate, E_H, is assumed to be approximately constant over the entire wall height, H, and acts even when the river is not in contact with the valley wall. In this case, the total amount of laterally supplied sediment for a cross section is given by:

$$q_s = E_R hP + E_H H. \tag{5}$$

E_H is likely a function of climatic boundary conditions (e.g., rainfall rate and frequency, temperature, etc.) (e.g., Bookhagen & Strecker, 2012; Hales & Roering, 2005), hillslope-material properties (degree of cementation, grain size, vegetation cover) (e.g., Acosta et al., 2015; Neely & DiBiase, 2020), and hillslope gradient (e.g., Roering et al., 1999), and is assumed to be constant as long as those conditions persist.

Lateral valley-wall erosion by the river requires that the river is able to remove all of the sediment that is laterally supplied from hillslope erosion in order to come in contact with the adjacent wall. Any excess capacity can then be used to actively erode the river adjacent wall, such that

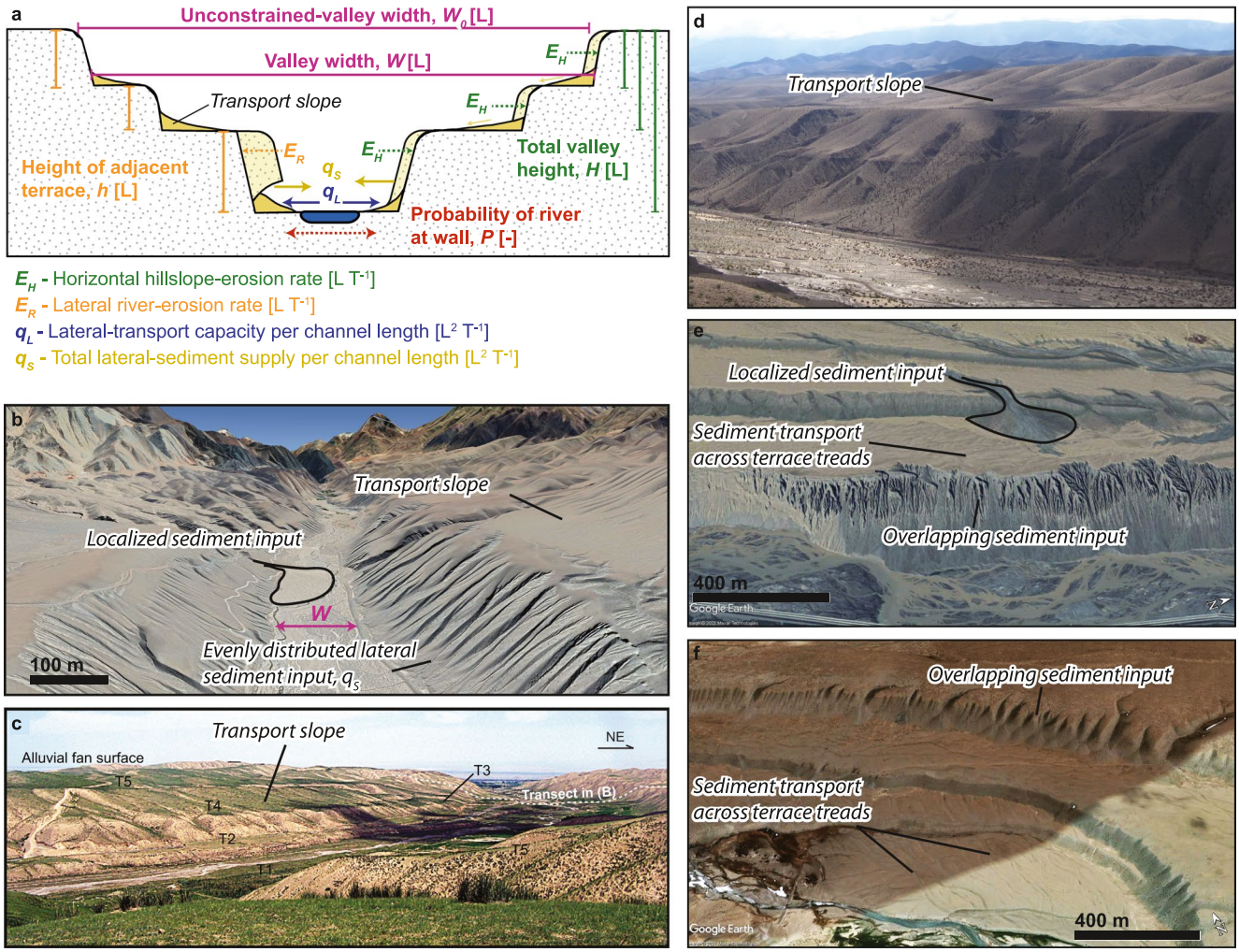

Figure 9. Schematic summary of proposed model and images of analyzed terraces. (a) Schematic model of a steady-state valley width in alluvial terrace systems. Valleys widen until the lateral sediment input, q_S, equals the evacuation of laterally supplied sediment by the river, q_L. (b–f) Google Earth and field images of a selection of analyzed terraces from sparsely vegetated regions to show evenly distributed lateral sediment input and gully structures allowing across-terrace sediment transport along transport slopes. Google Earth image (b) and field photo (d) of the Quebrada del Toro, Argentina (Tofelde et al., 2017), (c) field photo from Dahe river, Quilian Shan, Tibet, taken from original publication (Hu et al., 2017), (e) Google Earth image of Kuitun river, Tien Shan, China (Poisson & Avouac, 2004), and (f) Google Earth image from the Sutlej River, Tibet (Wang et al., 2017).

$$E_R h P = P q_L - E_H H. \tag{6}$$

The total valley-widening rate is the sum of both lateral river erosion and river-independent hillslope erosion. Each of the two processes dominates under different conditions. In cases when lateral sediment input is less than the ability of the river to remove sediment ($q_S < Pq_L$), both widening processes are active, but the majority of widening is achieved through lateral river erosion in times of wall contact. Combining this notion with Equation 6 yields:

$$\frac{dW}{dt} = E_H + E_R P = E_H + \frac{P q_L - E_H H}{hP} P \qquad \text{for } (q_S < P q_L). \tag{7}$$

In cases where the ability of the river to remove sediment is less than the lateral sediment input ($q_S > Pq_L$), the river is prevented from active wall erosion by sediment deposits at the wall toe, and wall-retreat rates are reduced to:

$$\frac{\mathrm{dW}}{\mathrm{dt}} = E_H \qquad \text{for } (q_S > P q_L). \tag{8}$$

In this case, even though valley walls retreat, the fluvial valley does not widen as long as that sediment is not removed from the toe of the walls.

Neither one of these two conditions, with Pq_L larger or smaller than q_S, results in the observed linear relationship between W and H after integration of the equation with respect to W. However, for the case that the rate of sediment removal by the river decreases to the rate of background hillslope supply, active undercutting of the river-adjacent valley wall ceases and a balance between hillslope-sediment supply, q_S, and lateral sediment removal by the river, q_L, emerges, which can be termed as a lateral sediment-flux steady-state. In such a case, Equations 7 and 8 will be equal and we have:

$$E_H = E_H + \frac{Pq_L - E_H H}{hP} P, \tag{9}$$

and rearranging this equation yields:

$$Pq_L = E_H H. \tag{10}$$

We describe the probability of the river to be at the valley side, P, as a function of the current valley width, W, and the unconstrained-valley width, W_0, or the width that a valley would evolve to in the absence of a valley wall (Figure 9a). We consider W_0 as similar to the channel-belt width, which comprises the active river channel(s) of width w_r, but also channel bars, abandoned channels and eroded, partially vegetated valley margins (Ashmore, 2013; Bertoldi et al., 2009; Limaye, 2020). Experimental data have shown that channel belts, even without lateral constraints, reach a quasi-equilibrium width and do not widen infinitely (e.g., Limaye, 2020). The river can move a lateral distance, d, within a certain time, Δt. The lateral distance, d, is the sum of two products: (a) the velocity at which the river moves laterally across the valley floor, V, times the probability that the river is located somewhere within the valley floor not touching the wall, $(1 - P)$, and (b) the river velocity once it hits the wall, v (which can be expected to be smaller than V), times the probability that it touches the wall, P:

$$d = V(1 - P)\Delta t + v\, P\, \Delta t. \tag{11}$$

In cases without lateral boundaries, that is, prior to any incision, $P = 0$ and hence:

$$d_{\text{no input}} = V\, \Delta t = W_0. \tag{12}$$

In cases of an existing wall and lateral sediment input, $P \neq 0$. Once the valley has reached a steady state, the lateral river velocity v decreases to zero, because otherwise the valley would continue to widen by river erosion. In this case, Equation 11 simplifies to:

$$d_{\text{input}} = V\,(1 - P)\,\Delta t = W_0\,(1 - P) = W. \tag{13}$$

When solving for P, this results in:

$$P = 1 - \frac{W}{W_0} = \frac{W_0 - W}{W_0}. \tag{14}$$

Our description of P thus varies from that of Hancock and Anderson (2002) and Martin et al. (2011), who expressed the probability term for the river to be located at the valley wall as the ratio of channel width to valley width, but without providing a derivation. Also, describing the probability of wall interaction by the ratio of river-to-valley width works better for single-thread channels and less well for multi-thread channels, which can be observed in some of the terrace sites.

Implementing Equation 14 into Equation 10 yields:

$$\frac{W_0 - W}{W_0} q_L = E_H H. \tag{15}$$

Solving for W yields a negative linear relationship between W and H:

$$W = W_0 - \frac{E_H W_0}{q_L} H. \tag{16}$$

Equation 16 describes a linear relationship between W and H, and thus is able to reproduce the (near-)linear trends between W and H observed in the field data. The slopes of the field data linear regression vary between −7.1 and −106.3 (Table S4 in Supporting Information S1). According to our proposed model, the differences in regression slopes are the result of locally different hillslope-erosion rates, E_H, lateral river-transport capacities, q_L, and unconstrained-valley widths, W_0. We expect that two cross sections in the same river close to one another would result in similar W_0 values, and W_0 values can theoretically be derived from the linear regression, as it equals the intercept with the y-axis. Even though the calculated regression intercepts at three sites for which more than one profile was published (Pazzaglia & Brandon, 2001; Ray & Srivastava, 2010; Wang et al., 2017) behave as expected (Table S4 in Supporting Information S1), the derived W_0 values cannot directly be compared. Most cross sections do not cover the entire valley wall on both sites, such that valley height values were measured relative to a reference surface or the highest displayed terrace (see Section 3.1). In those cases, valley height is systematically under-estimated. A constant shift of all datapoints within one data set to higher valley height values would result in lower W_0 values (Figure 5c).

In summary, we propose that hillslope-sediment supply, which scales linearly with valley height, H, sets the upper width to which valleys evolve by lateral river erosion. The river-adjacent terrace height, h, in turn, controls only the rate of widening as long as that upper limit width is not reached. Hence, given all other parameters to be constant, cycles in water discharge with constant amplitude and wavelength will result in paired river-terrace sequences, as the amount of lateral sediment supply from river-independent hillslope erosion increases with each new terrace level and, thus, reduces the width to which the active valley floor can widen. Importantly, neither of the two widening processes alone, lateral river erosion and river-independent hillslope erosion, would result in the observed linear W-H relationship (Figure 5c). Only if both processes are considered, and if we assume that alluvial rivers self-adjust to a lateral sediment-flux steady-state, can the observed linearity be reproduced.

5.2. Model Assumptions, Implications, and Future Work

Our proposed model predicts a relationship between valley width, W, and valley height, H, for a given river-independent hillslope-erosion rate, E_H, lateral-transport capacity, q_L, and unconstrained-valley width, W_0. As such, the model is not limited to alluvial terrace sequences. However, in order to explain the existence of paired terraces formed under constant climate cycles and to achieve a negative linear W-H relationship as observed for the special field settings, some assumptions must be fulfilled. First, a linear W-H relationship requires that the majority of sediment eroded at risers of higher terrace levels is not trapped on the terrace treads, but transported across terrace surfaces to the active floodplain. This sediment transport can be explained by the development of river-perpendicular transport slopes along several small gullies (Figures 9b–9f). To our knowledge, no study has measured sediment flux out of terraces levels in enough detail to test this assumption. Second, similar to previous studies (Blum et al., 2013; Bufe et al., 2019; Hancock & Anderson, 2002; Malatesta et al., 2017; Martin et al., 2011), we describe valley-width evolution only for a 1D cross section. Hence, the proposed relationship between W and H, as given in Equation 16, only applies to a segment of the river in which q_L and q_S are constant along the length of the valley. In the case of fluvial terraces, no well-developed drainage system is typically present on the terrace flats. Instead, the transport across terrace surfaces along small gullies ensures an approximately even sediment supply along the valley (Figures 9b, 9e, and 9f). Punctual lateral sediment input from tributaries, larger gullies or alluvial fans (Figures 9b and 9e) often affects the river system for some distance downstream. It remains unclear how uneven lateral sediment supply would have to be in order to cause the model to break down. We think that as long as the downstream effect of localized inputs spatially overlap, longitudinal variations in valley width will even out on the scale of a valley stretch. Third, we assume roughly constant E_H values across the entire height of the valley wall. Currently, to our knowledge, no data set exists to test this assumption either. Hence, this assumption must be tested in future work. Fourth, following Equation 16, a linear W-H relationship only emerges when each terrace step is formed under similar lateral-transport capacities, q_L. We note that this does not imply constant values of q_L through time. As q_L is thought to scale with upstream water discharge (Bufe et al., 2019; Wickert et al., 2013), upstream sediment supply (Constantine et al., 2014; Dunne et al., 2010), along-profile river gradient (Hancock & Anderson, 2002; Langston & Tucker, 2018; Suzuki, 1982), and planform curvature of river bends (Finnegan & Dietrich, 2011; Howard & Knutson, 1984; Langston & Tucker, 2018; Limaye & Lamb, 2014), q_L likely varies through time as climate or tectonic boundary conditions change. However, as long as those changes are cyclic (variations around a constant mean) and each terrace is formed under comparable boundary conditions to the previous ones, a linear W-H relationship emerges from the model. In contrast, in case

of a directed shift in tectonic or climatic boundary conditions, our model predicts a deviation from the linear *W-H* relationship. For example, for the terrace sequence in the Kuitun river, China, we have only analyzed terraces >6 ka, due to the change in the hydrological regime post 6 ka (Poisson & Avouac, 2004). If we include the width of the modern floodplain (measured in Google Earth), which formed under different hydrological conditions, the *W-H* linearity is reduced and the R^2 decreases from 0.99 to 0.81. Last, Equation 16 describes the equilibrium point between *W* and *H* for when the lateral river-erosion rate, E_R, is reduced to zero. Nevertheless, valleys slowly continue to widen at the rate of the river-independent hillslope-erosion rate, E_H. As long as E_H is constant with height, this continuous widening will shift all datapoints parallel to the *y*-axis in Figure 5c, but it will not affect the linear relationship between *W* and *H*.

Terrace sequences are thought to form due to alternating phases of vertical river incision and lateral erosion of valley walls (Bridgland & Westaway, 2008; Bull, 1990; Gilbert, 1877; Hancock & Anderson, 2002; Pazzaglia, 2013). However, in reality, both vertical river incision and lateral erosion may be active simultaneously, but dominant at different times (Li et al., 2021). The model, as described by Equation 16, does not explicitly account for vertical incision. Bufe et al. (2016) suggested that valleys during times of incision evolve to a steady width that is set by a balance between the lateral-transport capacity, q_L, and the "vertical" sediment supply from incision. Thus, self-organization of valley width from both lateral and vertical sediment-flux steady-state could, in principle, be implemented through the single parameter of lateral-transport capacity, q_L. In other words, vertical incision can be included as a fraction of the lateral-transport capacity. However, a linear *W-H* relationship requires that the fraction is comparable at times of terrace formation.

Our proposed model reproduces the first-order linear trend observed in measured paired terrace sequences (Figure 5c), and describes how valley width decreases linearly with valley height (Equation 16) under otherwise constant conditions. Paired terrace sequences were studied here, because they preserve past valley geometries. However, the model might be generally applicable anywhere where valleys are limited by a balance between lateral sediment supply and sediment removal by the river, rather than by the detachment of rock. Such a general applicability of the model has to be tested against independent data from valleys without terrace sequences and in non-alluvial settings. The model contains parameters that can be directly measured in the field, or can be estimated from measurable field parameters. We are not aware of existing datasets, in which all model-relevant parameters have been quantified. We found two datasets from the French Alps (Langston & Temme, 2019) and the Atacama Desert (Zavala et al., 2021) that allowed a first-order test of the model (Supporting Information S1). However, we note that both datasets only constrained some of the required parameters and both are located in bedrock settings. Analyses of the two datasets did not falsify our proposed model. Despite any limitations complicating the model evaluation, both datasets instead support that valley height appears to be a control parameter on valley width in addition to water discharge (or drainage area) and lithology. The general agreement between the two datasets and our model might suggest that some of the processes included in our model for alluvial valleys might also apply to bedrock settings.

In summary, our proposed model is a first attempt to explain the observed linear *W-H* relationship in alluvial terrace sequences. It is consistent with field observations and it is able to reproduce the formation of paired terrace sequences under cyclic climate forcing with a constant amplitude and wavelength. Future work is required to investigate our model assumptions in more detail in the field, and to compile datasets that quantify all model parameters to allow an independent test of the model.

6. Conclusions

The formation of paired river terraces requires valley narrowing, and our data compilation suggests that valley width, at least in weakly consolidated sedimentary terraces, is inversely proportional to valley height. This observation implies that valley height, or a parameter that scales linearly with valley height, controls valley width in addition to water discharge and lithology. We propose that lateral sediment input from hillslope-erosion processes limits the width to which alluvial valleys can widen, such that valleys widen until the lateral-transport capacity of the river matches the lateral, river-independent sediment input from hillslopes. Further research is required to comprehensively test the model and its assumptions against independent datasets and to investigate whether hillslope-sediment input impacts valley width evolution in non-terrace settings or in bedrock lithologies.

Unlike previous models, our model is able to explain the existence of paired terrace sequences formed under cyclic climate forcing. Currently, a limited number of existing numerical models have implemented lateral erosion and valley widening, as well as lateral sediment supply from collapse of wall material adjacent to the river valley. The concept of a balance between the lateral-transport capacity and sediment supply can, in principle, be easily included in such models.

The lateral-transport capacity likely scales dominantly with water discharge, indicating that knowledge of valley geometry (width, height, and slope), sediment size, and valley-wall retreat-rates can be used to back-calculate river discharge at the time of valley formation, which can serve as an indicator of paleo climate. As such, our model opens a door into climate reconstruction throughout Earth's history using valley shape.

Conflict of Interest

The authors declare no conflicts of interest relevant to this study.

Data Availability Statement

All data are available in the main text or the Supporting Information S1. Alternatively, the terrace height and width measurements (Data Set S1) can be accessed through the GFZ Data Services https://doi.org/10.5880/fidgeo.2022.021 (Tofelde et al., 2022).

Acknowledgments
The Deutsches Zentrum für Luft- und Raumfahrt (DLR) provided 12 m TanDEM-X DEM coverage of the Río Toro catchment via proposal DEM_GEOL1915 awarded to ST. AB received funding from the European Union's Horizon 2020 research and innovation programme under the Marie Sklodowska-Curie Research Fellowship (No. 841663). The authors would like to thank Abigail Langston and Valeria Zavala for providing additional data for a first-order test of our proposed model. The authors thank Mike Kirkby, Mikael Attal, Prakash Pokhrel, and one anonymous reviewer for their constructive feedback. Open Access funding enabled and organized by Projekt DEAL.

References

Acosta, V. T., Schildgen, T. F., Clarke, B. A., Scherler, D., Bookhagen, B., Wittmann, H., et al. (2015). Effect of vegetation cover on millennial-scale landscape denudation rates in East Africa. *Lithosphere*, *7*(4), 408–420. https://doi.org/10.1130/L402.1

Ahnert, F. (1998). *Introduction to geomorphology*. John Wiley & Sons Inc.

Ashmore, P. (2013). Morphology and dynamics of braided rivers.

Baynes, E. R. C., Lague, D., & Kermarrec, J. (2018). Supercritical river terraces generated by hydraulic and geomorphic interactions. *Geology*, *46*(6), 1–4. https://doi.org/10.1130/G40071.1

Bertoldi, W., Zanoni, L., & Tubino, M. (2009). Planform dynamics of braided streams. *Earth Surface Processes and Landforms*, *34*(4), 547–557. https://doi.org/10.1002/esp.1755

Blum, M., Martin, J., Milliken, K., & Garvin, M. (2013). Paleovalley systems: Insights from Quaternary analogs and experiments. *Earth-Science Reviews*, *116*(1), 128–169. https://doi.org/10.1016/j.earscirev.2012.09.003

Bookhagen, B., Fleitmann, D., Nishiizumi, K., Strecker, M. R., & Thiede, R. C. (2006). Holocene monsoonal dynamics and fluvial terrace formation in the northwest Himalaya, India. *Geology*, *34*(7), 601–604. https://doi.org/10.1130/G22698.1

Bookhagen, B., & Strecker, M. R. (2012). Spatiotemporal trends in erosion rates across a pronounced rainfall gradient: Examples from the southern Central Andes. *Earth and Planetary Science Letters*, *327*, 97–110. https://doi.org/10.1016/j.epsl.2012.02.005

Bridgland, D., & Westaway, R. (2008). Climatically controlled river terrace staircases: A worldwide Quaternary phenomenon. *Geomorphology*, *98*(3–4), 285–315. https://doi.org/10.1016/j.geomorph.2006.12.032

Brocard, G. Y., & Van der Beek, P. A. (2006). Influence of incision rate, rock strength, and bedload supply on bedrock river gradients and valley-flat widths: Field-based evidence and calibrations from western Alpine rivers (southeast France). In S. D. Willett, N. Hovius, M. T. Brandon, & D. M. Fisher (Eds.), *Tectonics, Climate, and Landscape Evolution* (Vol. 398, pp. 101–126). Special Papers, Geological Society of America.

Bruthans, J., Soukup, J., Vaculikova, J., Filippi, M., Schweigstillova, J., Mayo, A. L., et al. (2014). Sandstone landforms shaped by negative feedback between stress and erosion. *Nature Geoscience*, *7*(8), 597–601. https://doi.org/10.1038/ngeo2209

Bufe, A., Paola, C., & Burbank, D. W. (2016). Fluvial bevelling of topography controlled by lateral channel mobility and uplift rate. *Nature Geoscience*, *9*(9), 706–710. https://doi.org/10.1038/ngeo2773

Bufe, A., Turowski, J. M., Burbank, D. W., Paola, C., Wickert, A. D., & Tofelde, S. (2019). Controls on the lateral channel-migration rate of braided channel systems in coarse non-cohesive sediment. *Earth Surface Processes and Landforms*, *44*(14), 2823–2836. https://doi.org/10.1002/esp.4710

Bull, W. B. (1990). Stream-terrace Genesis: Implications for soil development. *Geomorphology*, *3*(3–4), 351–367. https://doi.org/10.1016/0169-555X(90)90011-E

Bull, W. B. (1991). Geomorphic responses to climatic change.

Colombo, F., Busquets, P., Ramos, E., Vergés, J., & Ragona, D. (2000). Quaternary alluvial terraces in an active tectonic region: The San Juan River Valley, Andean Ranges, San Juan Province, Argentina. *Journal of South American Earth Sciences*, *13*(7), 611–626. https://doi.org/10.1016/S0895-9811(00)00050-X

Constantine, J. A., Dunne, T., Ahmed, J., Legleiter, C., & Lazarus, E. D. (2014). Sediment supply as a driver of river meandering and floodplain evolution in the Amazon Basin. *Nature Geoscience*, *7*(12), 899–903. https://doi.org/10.1038/ngeo2282

Dunne, T., Constantine, J. A., & Singer, M. (2010). The role of sediment transport and sediment supply in the evolution of river channel and floodplain complexity. *Transactions - Japanese Geomorphological Union*, *31*(2), 155–170.

Finnegan, N. J., & Dietrich, W. E. (2011). Episodic bedrock strath terrace formation due to meander migration and cutoff. *Geology*, *39*(2), 143–146. https://doi.org/10.1130/G31716.1

Frankel, K. L., Pazzaglia, F. J., & Vaughn, J. D. (2007). Knickpoint evolution in a vertically bedded substrate, upstream-dipping terraces, and Atlantic slope bedrock channels. *Geological Society of America Bulletin*, *119*(3/4), 476–486. https://doi.org/10.1130/B25965.1

Gilbert, G. K. (1877). *Geology of the Henry Mountains*. US Government Printing Office.

Hales, T. C., & Roering, J. J. (2005). Climate-controlled variations in scree production, Southern Alps, New Zealand. *Geology*, *33*(9), 701–704. https://doi.org/10.1130/G21528.1

Hancock, G. S., & Anderson, R. S. (2002). Numerical modeling of fluvial strath-terrace formation in response to oscillating climate. *Bulletin of the Geological Society of America*, *114*(9), 1131–1142. https://doi.org/10.1130/0016-7606(2002)114<1131:NMOFST>2.0.CO

Hilton, R. G., & West, A. J. (2020). Mountains, erosion and the carbon cycle. *Nature Reviews Earth & Environment*, *1*(6), 284–299. https://doi.org/10.1038/s43017-020-0058-6

Howard, A. D., & Knutson, T. R. (1984). Sufficient conditions for river meandering: A simulation approach. *Water Resources Research*, *20*(11), 1659–1667. https://doi.org/10.1029/WR020i011p01659

Hu, X., Pan, B., Fan, Y., Wang, J., Hu, Z., Cao, B., et al. (2017). Folded fluvial terraces in a young, actively deforming intramontane basin between the Yumu Shan and the Qilian Shan mountains, NE Tibet. *Lithosphere*, *9*(4), 545–560. https://doi.org/10.1130/L614.1

Hurst, M. D., Mudd, S. M., Walcott, R., Attal, M., & Yoo, K. (2012). Using hilltop curvature to derive the spatial distribution of erosion rates. *Journal of Geophysical Research*, *117*, 1–19. https://doi.org/10.1029/2011JF002057

Lane, E. W. (1955). Importance of fluvial morphology in hydraulic engineering. *Proceedings of the American Society of Civil Engineers*, *81*(745).

Langston, A. L., & Temme, A. J. A. M. (2019). Impacts of lithologically controlled mechanisms on downstream bedrock Valley Widening. *Geophysical Research Letters*, *46*(21), 12056–12064. https://doi.org/10.1029/2019GL085164

Langston, A. L., & Tucker, G. E. (2018). Developing and exploring a theory for the lateral erosion of bedrock channels for use in landscape evolution models. *Earth Surface Dynamics*, *6*(1), 1–27. https://doi.org/10.5194/esurf-6-1-2018

Li, T., Venditti, J. G., & Sklar, L. S. (2021). An analytical model for lateral erosion from saltating bedload particle impacts. *Journal of Geophysical Research: Earth Surface*, *126*, 1–25. https://doi.org/10.1029/2020jf006061

Limaye, A. B. S. (2020). How do braided rivers grow channel belts? *Journal of Geophysical Research: Earth Surface*, *125*, 1–24. https://doi.org/10.1029/2020JF005570

Limaye, A. B. S., & Lamb, M. P. (2014). Numerical simulations of bedrock valley evolution by meandering rivers with variable bank material. *Journal of Geophysical Research: Earth Surface*, *119*, 927–950. https://doi.org/10.1002/2013JF002871.Received

Lisiecki, L. E., & Raymo, M. E. (2005). A Pliocene-Pleistocene stack of 57 globally distributed benthic δ 18 O records. *Paleoceanography*, *20*(1), 1–17. https://doi.org/10.1029/2004PA001071

Mackin, J. H. (1937). Erosional history of the big horn basin, Wyoming. *Bulletin of the Geological Society of America*, *48*(6), 813–894. https://doi.org/10.1130/gsab-48-813

Macklin, M. G., & Lewin, J. (2015). The rivers of civilization. *Quaternary Science Reviews*, *114*, 228–244. https://doi.org/10.1016/j.quascirev.2015.02.004

Maddy, D., Bridgland, D., & Westaway, R. (2001). Uplift-driven valley incision and climate-controlled river terrace development in the Thames Valley, UK. *Quaternary International*, *79*(1), 23–36. https://doi.org/10.1016/s1040-6182(00)00120-8

Malatesta, L. C., Prancevic, J. P., & Avouac, J. P. (2017). Autogenic entrenchment patterns and terraces due to coupling with lateral erosion in incising alluvial channels. *Journal of Geophysical Research: Earth Surface*, *122*, 335–355. https://doi.org/10.1002/2015JF003797

Marcotte, A. L., Neudorf, C. M., & Langston, A. L. (2021). Lateral bedrock erosion and valley formation in a heterogeneously layered landscape, Northeast Kansas. *Earth Surface Processes and Landforms*, *46*(11), 2248–2263. https://doi.org/10.1002/esp.5172

Martin, J., Cantelli, A., Paola, C., Blum, M., & Wolinsky, M. (2011). Quantitative modeling of the evolution and geometry of incised valleys. *Journal of Sedimentary Research*, *81*(1), 64–79. https://doi.org/10.2110/jsr.2011.5

May, C., Roering, J., Eaton, L. S., & Burnett, K. M. (2013). Controls on valley width in mountainous landscapes: The role of landsliding and implications for salmonid habitat. *Geology*, *41*(4), 503–506. https://doi.org/10.1130/G33979.1

Merritts, D. J., Vincent, K. R., & Wohl, E. E. (1994). Long river profiles, tectonism, and eustasy: A guide to interpreting fluvial terraces. *Journal of Geophysical Research*, *99*(B7), 14031–14050. https://doi.org/10.1029/94jb00857

Montgomery, D. R. (2002). Valley formation by fluvial and glacial erosion. *Geology*, *30*(11), 1047–1050. https://doi.org/10.1130/0091-7613(2002)030<1047:vfbfag>2.0.co;2

Neely, A. B., & DiBiase, R. A. (2020). Drainage area, bedrock fracture spacing, and weathering controls on landscape-scale patterns in surface sediment grain size. *Journal of Geophysical Research: Earth Surface*, *125*, 1–22. https://doi.org/10.1029/2020JF005560

Pazzaglia, F. J. (2013). Fluvial terraces. *Treatise on Geomorphology*, 379–412.

Pazzaglia, F. J., & Brandon, M. T. (2001). A fluvial record of long-term steady-state uplift and erosion across the Cascadia forearc high, western Washington State. *American Journal of Science*, *301*(4–5), 385–431. https://doi.org/10.2475/ajs.301.4-5.385

Perron, J. T., Kirchner, J. W., & Dietrich, W. E. (2009). Formation of evenly spaced ridges and valleys. *Nature*, *460*(7254), 502–505. https://doi.org/10.1038/nature08174

Poisson, B., & Avouac, J. (2004). Holocene hydrological changes inferred from Alluvial stream entrenchment in North Tian Shan (Northwestern China). *The Journal of Geology*, *112*(2), 231–249. https://doi.org/10.1086/381659

Ray, Y., & Srivastava, P. (2010). Widespread aggradation in the mountainous catchment of the Alaknanda-Ganga River System: Timescales and implications to Hinterland-foreland relationships. *Quaternary Science Reviews*, *29*(17–18), 2238–2260. https://doi.org/10.1016/j.quascirev.2010.05.023

Rigsby, C. A., Baker, P. A., & Aldenderfer, M. S. (2003). Fluvial history of the Rio Ilave valley, Peru, and its relationship to climate and human history. *Palaeogeography, Palaeoclimatology, Palaeoecology*, *194*(1–3), 165–185. https://doi.org/10.1016/S0031-0182(03)00276-1

Roering, J. J., Kirchner, J. W., & Dietrich, W. E. (1999). Evidence for nonlinear, diffusive sediment transport on hillslopes and implications for landscape morphology. *Water Resources Research*, *35*(3), 853–870. https://doi.org/10.1029/1998WR900090

Schanz, S. A., & Montgomery, D. R. (2016). Lithologic controls on valley width and strath terrace formation. *Geomorphology*, *258*, 58–68. https://doi.org/10.1016/j.geomorph.2016.01.015

Schanz, S. A., Montgomery, D. R., Collins, B. D., & Duvall, A. R. (2018). Multiple paths to straths: A review and reassessment of terrace Genesis. *Geomorphology*, *312*, 12–23. https://doi.org/10.1016/j.geomorph.2018.03.028

Scherler, D., Bookhagen, B., Wulf, H., Preusser, F., & Strecker, M. R. (2015). Increased late Pleistocene erosion rates during fluvial aggradation in the Garhwal Himalaya, northern India. *Earth and Planetary Science Letters*, *428*, 255–266. https://doi.org/10.1016/j.epsl.2015.06.034

Shobe, C. M., Tucker, G. E., & Anderson, R. S. (2016). Hillslope-derived blocks retard river incision. *Geophysical Research Letters*, *43*(10), 5070–5078. https://doi.org/10.1002/2016GL069262

Suzuki, T. (1982). Rate of lateral planation by Iwaki River, Japan. *Transactions - Japanese Geomorphological Union*, *3*(1), 1–24.

Tao, Y., Xiong, J., Zhang, H., Chang, H., & Li, L. (2020). Climate-driven formation of fluvial terraces across the Tibetan Plateau since 200 kya: A review. *Quaternary Science Reviews*, *237*, 106303. https://doi.org/10.1016/j.quascirev.2020.106303

Tofelde, S., Bufe, A., & Turowski, J. M. (2022). *River terrace height and width analysis*. GFZ Data Services. https://doi.org/10.5880/fidgeo.2022.021

Tofelde, S., Savi, S., Wickert, A. D., Bufe, A., & Schildgen, T. F. (2019). Alluvial channel response to environmental perturbations: Fill-terrace formation and sediment-signal disruption. *Earth Surface Dynamics*, *7*, 609–631. https://doi.org/10.5194/esurf-2018-84

Tofelde, S., Schildgen, T. F., Savi, S., Pingel, H., Wickert, A. D., Bookhagen, B., et al. (2017). 100 kyr fluvial cut-and-fill terrace cycles since the Middle Pleistocene in the southern Central Andes, NW Argentina. *Earth and Planetary Science Letters*, *473*, 141–153. https://doi.org/10.1016/j.epsl.2017.06.001

Tomkin, J. H., Brandon, M. T., Pazzaglia, F. J., Barbour, J. R., & Willett, S. D. (2003). Quantitative testing of bedrock incision models for the Clearwater River, NW Washington State. *Journal of Geophysical Research*, *108*(B6), 2308. https://doi.org/10.1029/2001JB000862

Tucker, G. E., & Slingerland, R. (1997). Drainage basin responses to climate change. *Water Resources Research*, *33*(8), 2031–2047. https://doi.org/10.1029/97WR00409

Tucker, G. E., & Whipple, K. X. (2002). Topographic outcomes predicted by stream erosion models: Sensitivity analysis and intermodel comparison. *Journal of Geophysical Research*, *107*(B9), ETG1–ETG16. https://doi.org/10.1029/2001jb000162

Van den Berg, M. W., & van Hoof, T. (2001). The maas terrace sequence at Maastricht, SE Netherlands: Evidence for 200 m of late Neogene and Quaternary surface uplift. *River Basin Sediment Systems: Archives of Environmental Change*, 45–86.

Vandenberghe, J. (2002). The relation between climate and river processes, landforms and deposits. *Quaternary International*, *91*(1), 17–23. https://doi.org/10.1016/S1040-6182(01)00098-2

Wang, Z., Meyer, M. C., Gliganic, L. A., Hoffmann, D. L., & May, J. H. (2017). Timing of fluvial terrace formation and concomitant travertine deposition in the upper Sutlej River (Tirthapuri, southwestern Tibet) and paleoclimatic implications. *Quaternary Science Reviews*, *169*, 357–377. https://doi.org/10.1016/j.quascirev.2017.06.009

Wickert, A. D., Martin, J. M., Tal, M., Kim, W., Sheets, B., & Paola, C. (2013). River channel lateral mobility: Metrics, time scales, and controls. *Journal of Geophysical Research: Earth Surface*, *118*, 396–412. https://doi.org/10.1029/2012JF002386

Wickert, A. D., & Schildgen, T. F. (2019). Long-profile evolution of transport-limited gravel-bed rivers. *Earth Surface Dynamics*, *7*(1), 17–43. https://doi.org/10.5194/esurf-7-17-2019

Willett, S. D., McCoy, S. W., Perron, J. T., Goren, L., Chen, C. Y., Perron, J. T., et al. (2014). Dynamic reorganization of river basins. *Science*, *343*(6175), 1248765. https://doi.org/10.1126/science.1248765

Zavala, V., Carretier, S., Regard, V., Bonnet, S., Riquelme, R., & Choy, S. (2021). Along-stream variations in valley flank Erosion rates measured using 10Be concentrations in colluvial deposits from Canyons in the Atacama Desert. *Geophysical Research Letters*, *48*(5), 1–11. https://doi.org/10.1029/2020GL089961